Journal of Catalysis 282 (2011) 191–200

Contents lists available at ScienceDirect

Journal of Catalysis

journal homepage: www.elsevier.com/locate/jcat

Direct oxidation of methanol to formaldehyde by N_2O on $[Fe]^{1+}$ and $[FeO]^{1+}$ sites in Fe–ZSM-5 zeolite: A density functional theory study

Mehmet Ferdi Fellah

Department of Chemical Engineering, Yuzuncu Yil University, Van 65080, Turkey

ARTICLE INFO

Article history:
Received 15 April 2011
Revised 31 May 2011
Accepted 13 June 2011
Available online 20 July 2011

Keywords:
DFT
Methanol oxidation
Formaldehyde
N_2O
Iron site
Fe–ZSM-5
MFI

ABSTRACT

Density functional theory (DFT) calculations were carried out in a study of the mechanism of direct oxidation of methanol to formaldehyde by N_2O over an extra-framework species in ZSM-5 zeolite represented by a $[(SiH_3)_4AlO_4(Fe)$ or $(FeO)]$ cluster models. The major difference between these two sites is that in the case of the $[Fe]^{1+}$ site, a reaction is present that leads to the formation of the thermodynamically highly stable grafted OH and methoxy (OCH_3) species. Moreover, the vibrational frequencies for grafted species on the surface match well with the experimental values. The theoretical calculations achieved in this study obviously show that $[Fe–O]^{1+}$ site in Fe–ZSM-5 catalyst has a significant role on the catalytic oxidation of methanol to formaldehyde by N_2O.

1. Introduction

Methanol, the smallest number of aliphatic alcohols, has traditionally been used as a solvent and as a feedstock for bulk organic chemicals (primarily formaldehyde), with modest growth potential [1]. Forty percent of the produced methanol is used to form formaldehyde on iron molybdenum oxide catalysts. Because of its relatively low cost, high purity, and variety of chemical reactions, formaldehyde has become one of the world's most important industrial and research chemicals [2]. Formaldehyde is currently produced directly from methanol via two different ways such as dehydrogenation or oxidative dehydrogenation on Ag or Cu catalysts and oxidation with Fe-containing MoO_3 catalysts. These processes need high temperature (573–923 K) and produce several by-products such as carbon monoxide, carbon dioxide, dimethyl ether, methyl formate, and formic acid [2]. There has been significant research activity to develop new processes for producing formaldehyde. In the literature, there are a few theoretical studies [3–6] on methanol oxidation to formaldehyde with small iron-oxo species. Liang et al. [7] have investigated several reactions of methanol oxidation to formaldehyde on $[FeO]^{1+}$–ZSM-5 modeled as $[(SiH_3)_2AlO_2(OH)_2(FeO)]$ in their theoretical study where direct oxidation of methane on Fe–ZSM-5 zeolite has been studied. However neither theoretical nor experimental literature has an investigation for methanol oxidation to formaldehyde by N_2O on Fe–ZSM-5 zeolite.

Fe-exchanged ZSM-5 catalysts have good catalytic activities for a number of reactions. It has been experimentally reported [8,9] that [Fe,Al]MFI gives good performance in the selective oxidation of benzene to phenol. The α-form of oxygen (extra-framework oxygen) formed by decomposition of N_2O plays an important role in the direct oxidation of benzene on Fe–ZSM-5 that is confirmed by both experimental [10–15] and theoretical [16–20] literature. It should also be noted that Fe–ZSM-5 is an active catalyst for the stoichiometric decomposition of N_2O to form α-oxygen, according to both experimental [21–33] and theoretical [32–41] reports. Methanol selectivity is less than 2% at temperatures above 523 K for methanol formation reactions on Fe/Al-MFI via the oxidation of methane by nitrous oxide [42]. On the contrary, benzene is selectively oxidized to phenol by interaction with the α-form of the surface oxygen produced on Fe–ZSM-5 zeolite by N_2O decomposition [10–15,43]. The following reaction is proposed for the decomposition of N_2O to form α-oxygen [14,15,44]

$$N_2O + (\ )_\alpha \rightarrow (O)_\alpha + N_2 \quad (1)$$

The major challenge or debate in understanding the activity of Fe/ZSM-5 catalysts is about the nature of the active sites in the ZSM-5 zeolite [45]. Extra-framework Fe species in the zeolite micropores can be present as mono-, bi-, or oligonuclear cationic species; neutral iron oxide species; or mixed oxide phases combining Fe and Al. Several experimental studies have utilized extended X-ray

E-mail address: mffellah@gmail.com

0021-9517/$ - see front matter © 2011 Elsevier Inc. All rights reserved.
doi:10.1016/j.jcat.2011.06.012

absorption fine structure, high-resolution X-ray absorption near-edge spectroscopy, Fourier transform infrared spectroscopy, electron spin resonance, electron paramagnetic resonance, X-ray diffraction, Mössbauer spectroscopy, and UVvisible spectroscopy and have reported that iron sites of Fe–ZSM-5 are mononuclear sites [46–54], binuclear structures [53,55–59] and small iron oxide or oligomeric clusters [59–61]. Volodin et al. [54] studied the spin state of iron ions in Fe–ZSM-5 zeolites experimentally and reported that ferrous ions have integer electron spins ($S = 2$). They also reported that Fe–ZSM-5 catalyst contains a FeO complex where iron has a charge of 3+. Based on an experimental [62] XAFS study, it was reported that FeO complexes where Fe atoms are in the 3+ and 4+ oxidation states exist in Fe–ZSM-5 catalyst. Several Fe–ZSM-5 clusters having different iron charges have been used in many theoretical studies. Yoshizawa et al. [19,63] oxidation to phenol on Fe–ZSM-5 zeolite represented as a $[(SiH_3)_2AlO_2(OH)_2(FeO)]$ cluster. Benzene oxidation to phenol by N_2O was also studied over $(SiH_3)_4AlO_4(FeO)$ and $(SiH_3)_4AlO_4(FeO_2)$ clusters [16]. Recently, computational studies investigated the direct benzene oxidation to phenol by N_2O on Fe^{1+}–ZSM-5 [64] zeolite represented as a $[Si_4AlO_4H_{12}Fe]$ cluster and on $[FeO]^{1+}$–ZSM-5 zeolite modeled as $[Si_4AlO_4H_{12}FeO]$ [65]. A $[Si_4AlO_4H_{12}Fe]$ cluster where Fe has a charge of 1+ was recently investigated for methane oxidation to methanol by N_2O [66]. A mononuclear Fe^{1+} in the Fe–ZSM-5 cluster has been investigated in many theoretical studies for several reactions [16,17,36,64,65,67].

As mentioned above, neither experimental nor theoretical analysis of methanol oxidation to formaldehyde by N_2O over the Fe–ZSM-5 catalyst has been performed. Therefore, the aim of this study is to analyze the catalytic reactivity on $[Fe]^{1+}$ and $[FeO]^{1+}$ sites in Fe–ZSM-5 zeolite during the catalytic oxidation of methanol to formaldehyde formation by nitrous oxide. Density functional theory (DFT) calculations with the B3LYP formalism using 6–31G(d,p) as a basis set for all atoms are utilized to obtain energy profiles, equilibrium geometries, and transition state geometries.

2. Surface model and calculation method

All calculations in this study were based on DFT [68] as implemented in the Gaussian suite of program [69]. Becke's three-parameter hybrid method [70,71] involving the Lee, Yang, and Parr correlation functional (B3LYP [72]) formalism was utilized to take into account the exchange and correlation. The 6–31G(d,p) basis set was used for all atoms including iron.

A cluster modeling approach in present study was used to simulate a representative portion of ZSM-5 zeolite stabilizing the extra-framework iron species. Previous studies on iron-modified ZSM-5 and ferrierite zeolites by Kachurovskaya et al. [20,73] reported only minor quantitative differences between the results obtained using cluster and periodic modeling approach. In addition, cluster modeling approach has been widely used to create a qualitative molecular-level picture of CO and NO adsorption on different iron sites of Fe–ZSM-5 [74]. Very similar structural and energetic properties of the adsorption complexes were obtained by using small 5T and large 83T ZSM-5 cluster models [74]. A more important issue is that DFT calculations on cluster or periodic zeolite models generally predict very similar reactivity trends [74–77]. On the other hand, one should make a calculation for methanol oxidation to formaldehyde on a larger cluster.

In this study, a ZSM-5 cluster including five Si and four O atoms was cut from inside a ZSM-5 channel constructed by using the Cartesian coordinates reported by Lermer et al. in a XRD study [78]. The Al atom was placed in the T12 site of the framework surrounded by O and Si atoms resulting in a $[(SiH_3)_4AlO_4]^{1-}$. The negative charge of the cluster was compensated by the extra-framework reactive $[Fe]^{1+}$ and $[FeO]^{1+}$ sites. The resulting cluster models are shown in Fig. 1. The dangling bonds of the terminal silicon atoms of all clusters were terminated with H atoms. All atoms of the cluster, except terminating H atoms, and the reactant and product molecules were kept relaxed. Terminating H atoms were kept fixed to orient in the T-O direction of the next Si site.

Energy profile, equilibrium geometry (EG), and transition state (TS) calculations were performed for the determination of the acti-

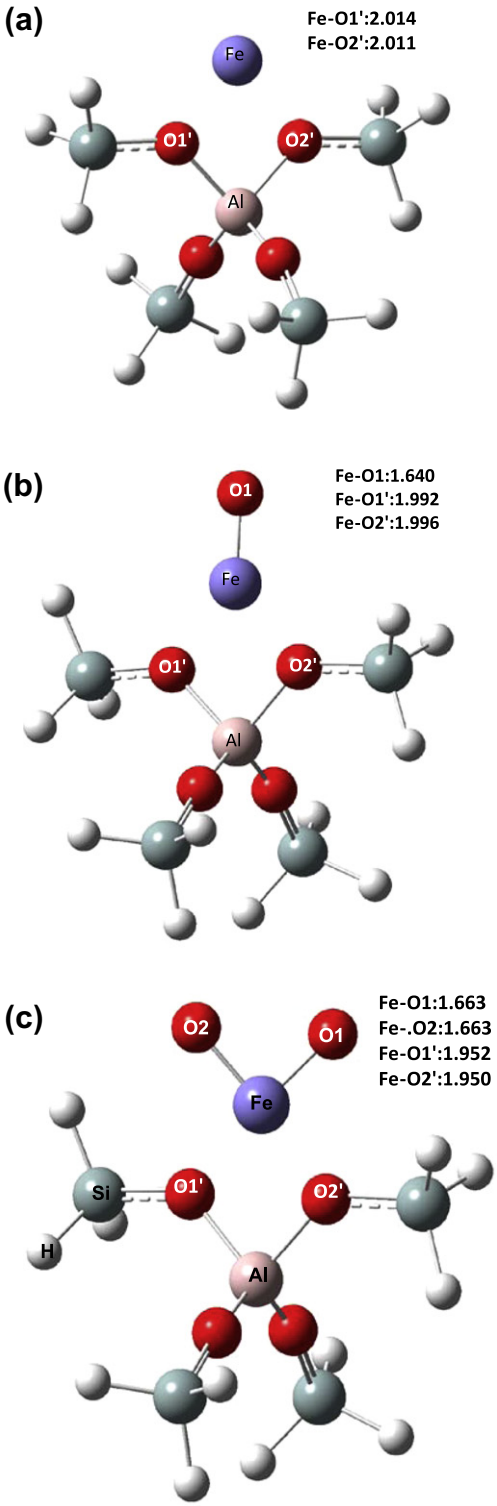

Fig. 1. Optimized geometries for (a) $[Fe]^{1+}$, (b) $[Fe–O]^{1+}$ and (c) $[O–Fe–O]^{1+}$ sites in Fe–ZSM-5 cluster (distance values in units of angstroms).

vation barriers and relative reaction energies. All energy values and energy differences in this study include zero-point energy (ZPE) corrections, which were obtained using frequency calculations at a temperature of 298 K because no experimental thermochemistry data are available for methanol oxidation to formaldehyde by N_2O on Fe–ZSM-5 catalyst. The computed $\langle S2 \rangle$ values confirmed that the spin contamination was very small (max. 0.19% after annihilation). Vibrational analysis was also performed to obtain vibrational frequencies and Gibbs free energies. All frequency values were scaled by 0.9613 [79] to reproduce experimental fundamentals. Time-dependent DFT calculations were performed to calculate UV–vis spectra. Mulliken population analysis [80] was utilized to obtain Mulliken atomic charges and Mulliken atomic spin densities. Natural bond orbital (NBO) [81] analysis was used to obtain electronic configurations of iron atoms. The convergence criteria involving gradients of maximum force, root-mean-square (rms) force, maximum displacement, and rms displacement in Gaussian software were 0.000450, 0.000300, 0.001800, and 0.001200, respectively.

The computational strategy employed in this study is as follows. Initially, the correct spin multiplicity (SM) of the system consisting of cluster and adsorbing molecules was determined by single point energy (SPE) calculations. SPEs were calculated with different SM numbers for each cluster system, and the SM number that corresponds to the lowest SPE was accepted as the correct SM. The cluster and the adsorbing molecules, N_2O and CH_3OH, were then fully optimized geometrically by means of EG calculations.

The adsorbing molecule was first located over the active site of the cluster at a selected distance, and a coordinate driving calculation was performed by selecting a reaction coordinate to obtain the variation of the relative energy with a decreasing reaction coordinate to get an energy profile as a function of the selected reaction coordinate distance. These energy profiles also helped us find TS and final EGs by using the geometry that has the highest energy and the geometry that has the final minimum energy, respectively. SPE calculations were also performed where necessary by locating the adsorbing molecule in the vicinity of the catalytic cluster. Coordinate driving calculations resulted in an energy profile. The resulting relative energies for the cluster and reactant molecule complex were plotted against the reaction coordinate. The relative energy was defined with the following formula:

$$\Delta E = E_{\text{System}} - (E_{\text{Cluster}} + E_{\text{Adsorbate}})$$

where E_{System} is the calculated energy of the optimized geometry containing the cluster and the adsorbing molecule (TS or EG), E_{Cluster} is the energy of the cluster, and $E_{\text{Adsorbate}}$ is that of the adsorbing molecule. After the energy profile was obtained for the reaction step, the geometry with the minimum energy on the energy profile was re-optimized by means of EG calculations to obtain the optimized geometry for the particular reaction step. In this re-optimization calculation, the reaction coordinate was not fixed. Additionally, the geometry with the highest energy from the energy profile was taken as the input geometry for the TS geometry calculations. Starting from these geometries, the TS structures with only one negative eigenvalue in Hessian matrix were obtained. TS geometries were calculated by using the Berny Algorithm [82] implemented in Gaussian software.

3. Results

3.1. Optimization of clusters

The optimized geometries for the Fe– and FeO–ZSM-5 clusters were obtained for the charge neutral cluster, and the SM corresponding to the lowest SPE was determined to be 6 (sextet) meaning there are five unpaired electrons. The SM number was also determined as 6 for the clusters including N_2O and methanol molecules. This value was used for all reactions studies. It means that the number of unpaired electrons was kept constant throughout all calculations with an even number of electrons to avoid spin transitions along the reaction path. The optimized geometries of clusters are depicted in Fig. 1. Si–O distances of a cluster range from 1.55 to 1.68 Å. The corresponding distances reported earlier in the experimental literature are between 1.55 and 1.65 Å [78].

3.2. Oxidation of methanol to formaldehyde by N_2O on the $[Fe]^{1+}$–ZSM-5 cluster

The following elementary reaction steps A1–A6 are considered to be involved in different potential reaction paths for the oxidation of methanol oxidation to formaldehyde by N_2O:

Step A1: N_2O decomposition

$$N_2O + Fe{-}ZSM5 \rightarrow Fe{-}O{-}ZSM5 + N_2 \quad (2)$$

Step A2: Methanol adsorption

$$Fe{-}O{-}ZSM5 + CH_3OH \rightarrow O{-}Fe{-}OHCH_3{-}ZSM5 \quad (3)$$

Step A3: Proton transfer from the OH to form grafted species

$$O{-}Fe{-}OHCH_3{-}ZSM5 \rightarrow HO{-}Fe{-}OCH_3{-}ZSM5 \quad (4)$$

Step A4: Proton transfer from metoxy to form formaldehyde and water

$$HO{-}Fe{-}OCH_3{-}ZSM5 \rightarrow H_2O{-}Fe{-}OCH_2{-}ZSM5 \quad (5)$$

Step A5: Desorption of water

$$H_2O{-}Fe{-}OCH_2{-}ZSM5 \rightarrow Fe{-}OCH_2{-}ZSM5 + H_2O \quad (6)$$

Step A6: Desorption of formaldehyde

$$CH_2O{-}Fe{-}ZSM5 \rightarrow Fe{-}ZSM5 + CH_2O \quad (7)$$

First reaction (step A1) of the catalytic cycle for oxidation of methanol to formaldehyde by N_2O on Fe^{1+}–ZSM-5 cluster is the decomposition of N_2O molecule resulting in Fe–O site on the ZSM-5 cluster. This step was investigated in our previous study [39]. The optimized geometry of [Fe–O]–ZSM-5 cluster is depicted in part b of Fig. 1. At the next step, methanol molecule adsorbs on the Fe center of [FeO] site (step A2). This exothermic reaction step (ΔE = −100 kJ/mol) occurs without an activation barrier. The corresponding optimized geometry is shown in Fig. 2.

Proton transfer from the OH group of adsorbed methanol to O atom of the extra-framework iron cluster results in the formation of adsorbed grafted species such as hydroxyl and methoxy (step A3). This reaction step is strongly favored thermodynamically (ΔE = −127 kJ/mol) and faces a relatively low activation barrier (E_{act} = 23 kJ/mol). TS and EG of this step are depicted in Fig. 3.

Subsequent proton transfer from the CH_3 group of adsorbed methoxy to adsorbed hydroxyl group in the extra-framework iron cluster results in formaldehyde and water formation (step A4). This reaction step is endothermic (ΔE = 142 kJ/mol) and shows a very high activation barrier (E_{act} = 155 kJ/mol). The energy profile for this step obtained by the coordinate driving calculation in Gaussian software is shown in Fig. 4a to illustrate the computational methodology used in this study. TS and EG for this step are represented in parts b and c of Fig. 4.

After these reactions, formaldehyde formed on the clusters or water will desorb from the surfaces. If formaldehyde firstly desorbs from the surface, desorption barrier value is calculated to be 138 kJ/mol. The desorption barrier is 81 kJ/mol if water

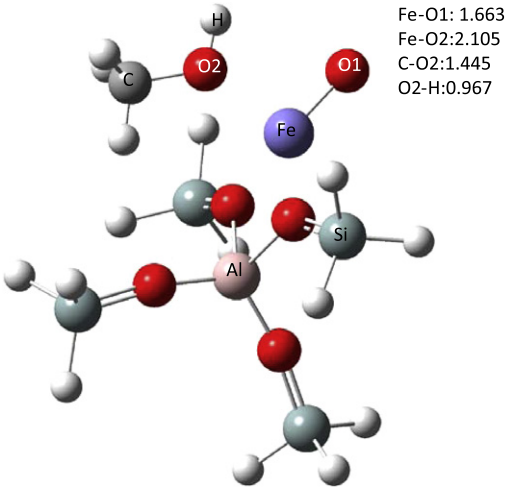

Fig. 2. Final equilibrium geometry for methanol adsorption (step A2) (distance values in units of angstroms).

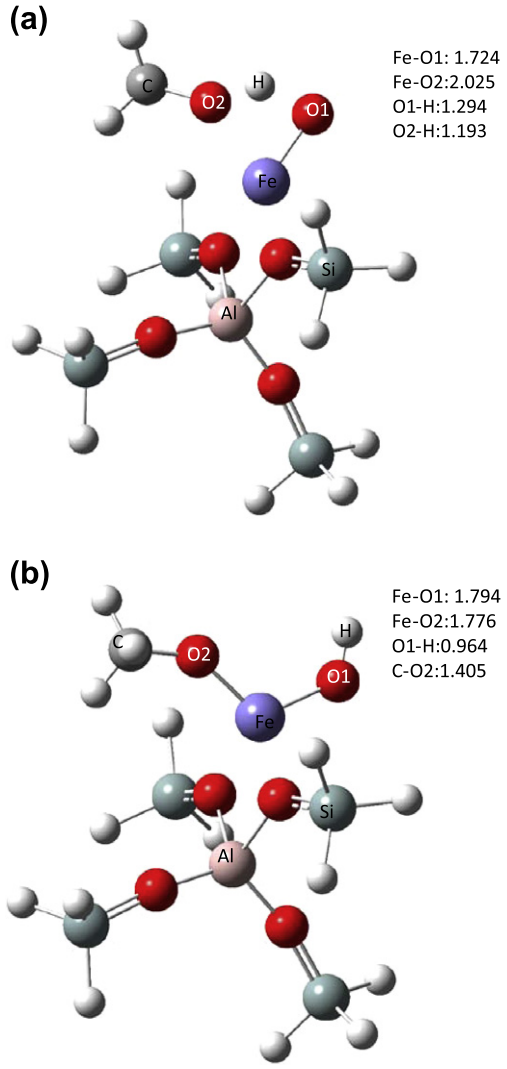

Fig. 3. (a) TS and (b) EG for proton transfer from the OH to form grafted species (step A3) (distance values in units of angstroms).

desorbs firstly from the surface. ΔG values for formaldehyde and water desorptions from the surface is computed as 102 and 35 kJ/mol, respectively. When water is absent on the surface, desorption barrier value for formaldehyde is computed as 127 kJ/mol.

3.3. Oxidation of methanol to formaldehyde by N_2O on the $[FeO]^{1+}$–ZSM-5 cluster

The following elementary steps B1–B7 are considered for direct methanol oxidation to formaldehyde by N_2O over $[FeO]^{1+}$.

Step B1: N_2O decomposition

$$N_2O + Fe{-}O{-}ZSM5 \rightarrow O{-}Fe{-}O{-}ZSM5 + N_2 \quad (8)$$

Step B2: Methanol adsorption

$$O{-}Fe{-}O{-}ZSM5 + CH_3OH \rightarrow O{-}O{-}Fe{-}OHCH_3{-}ZSM5 \quad (9)$$

Step B3a: Proton transfer from the OH to form grafted species

$$O{-}O{-}Fe{-}OHCH_3{-}ZSM5 \rightarrow HO{-}O{-}Fe{-}OCH_3{-}ZSM5 \quad (10)$$

Step B3b: Proton transfer from the OH to form grafted species

$$O{-}O{-}Fe{-}OHCH_3{-}ZSM5 \rightarrow O{-}OH{-}Fe{-}OCH_3{-}ZSM5 \quad (11)$$

Step B4: Proton transfer metoxy to form formaldehyde and water after step B3a

$$HO{-}O{-}Fe{-}OCH_3{-}ZSM5 \rightarrow H_2O{-}O{-}Fe{-}OCH_2{-}ZSM5 \quad (12)$$

Step B5: Proton transfer metoxy to form formaldehyde and water after step B3b

$$O{-}OH{-}Fe{-}OCH_3{-}ZSM5 \rightarrow O{-}H_2O{-}Fe{-}OCH_2{-}ZSM5 \quad (13)$$

Step B6: Desorption of formaldehyde

$$H_2O{-}O{-}Fe{-}OCH_2{-}ZSM5 \rightarrow O{-}Fe{-}H_2O{-}ZSM5 + CH_2O \quad (14)$$

Step B7: Desorption of water

$$H_2O{-}O{-}Fe{-}OCH_2{-}ZSM5 \rightarrow O{-}Fe{-}OCH_2{-}ZSM5 + H_2O \quad (15)$$

Similar to the case of the Fe^{1+}–ZSM-5, first reaction (step B1) of the catalytic cycle for oxidation of methanol to formaldehyde by N_2O on $(FeO)^{1+}$–ZSM-5 cluster is the decomposition of N_2O molecule resulting in O–Fe–O site on the ZSM-5 cluster. This step was also studied in our previous work [65]. The optimized geometry of [O–Fe–O]–ZSM-5 cluster is depicted in part c of Fig. 1.

The adsorption of methanol on $(OFeO)^{1+}$ site (step B2) is an exothermic reaction (ΔE = −82 kJ/mol). The corresponding TS and EG structures of the step, which occurred without an activation barrier, are shown in Fig. 5.

Proton transfer from the OH group of adsorbed methanol to one O atom of the extra-framework iron site of $(OFeO)^{1+}$ results in the formation of adsorbed grafted species such as hydroxyl and methoxy (step B3a). This reaction step is an endothermic reaction (ΔE = +72 kJ/mol) that takes place on the site with a relatively low activation barrier (E_{act} = 19 kJ/mol). $\Delta G^{\#}$ for this reaction is calculated to be 79 kJ/mol. TS and EG of this step are also depicted in Fig. 6.

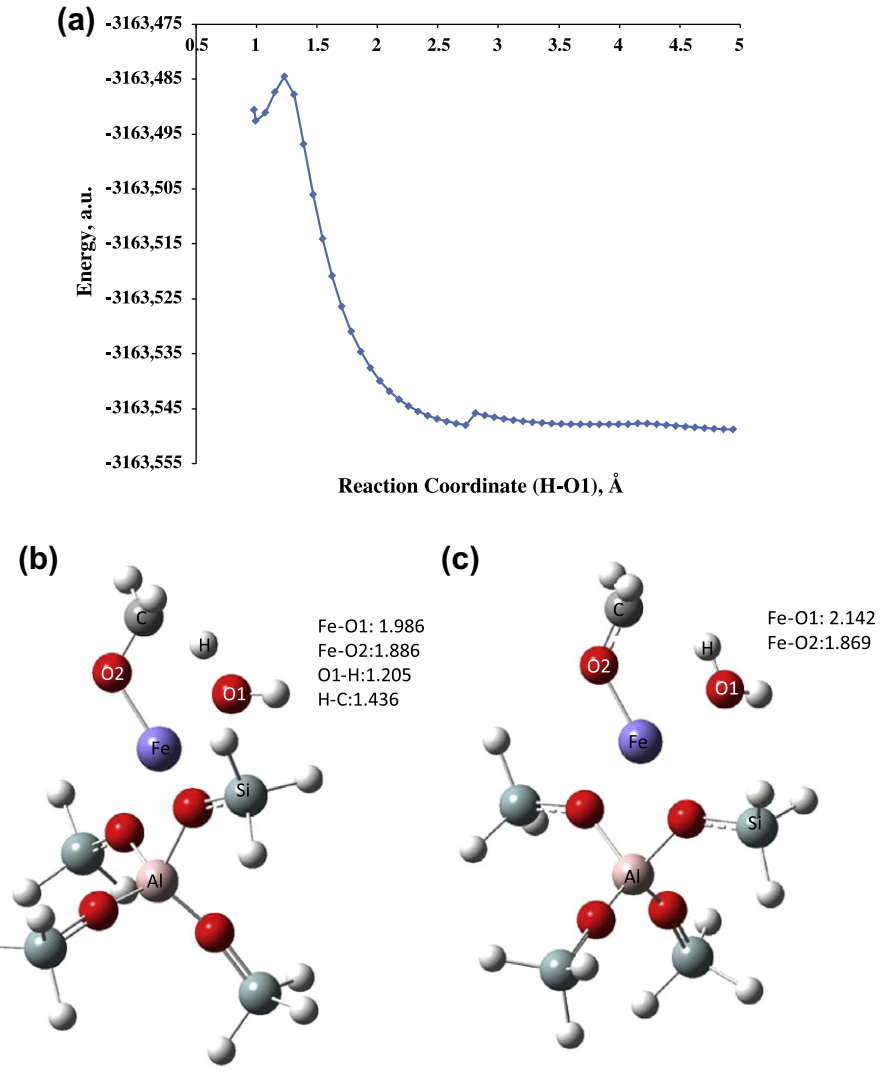

Fig. 4. (a) Energy profile, (b) TS, (c) EG proton transfer from CH_3 of metoxy to form formaldehyde and water (step A4) (distance values in units of angstroms).

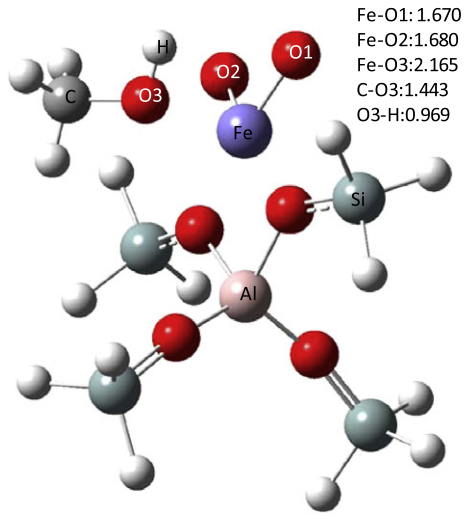

Fig. 5. Final equilibrium geometry for methanol adsorption (step B2) (distance values in units of angstroms).

Another alternative reaction path for the formation of grafted species is the hydrogen transfer to other oxygen atom of the iron site (step B3b). This reaction is also endothermic step (ΔE = +81 kJ/mol) with an activation barrier value of 22 kJ/mol. $\Delta G^{\#}$ for this reaction is computed as 84 kJ/mol. Fig. 7 represents the corresponding TS and EG structures of this step.

Following proton transfer from the CH_3 group of adsorbed methoxy to adsorbed hydroxyl group in the extra-framework iron cluster after step B3a results in formaldehyde and water formation (step B4). This reaction step is strongly favored thermodynamically (ΔE = −171 kJ/mol) and shows a very low activation barrier (E_{act} = 24 kJ/mol). Fig. 8 represents TS and EG structures for this step.

Another proton transfer from the CH_3 group of metoxy is step B5, which occurs after step B3b. Similar to previous reaction (step B4), this step is also strongly favored thermodynamically (ΔE = −177 kJ/mol) and shows a very low activation barrier (E_{act} = 22 kJ/mol). The corresponding TS and EG structures for this step are depicted in Fig. 9.

After these reactions, formaldehyde formed on the clusters or water will desorb from the surfaces to complete the catalytic cycle. If formaldehyde desorbs from the surface, desorption barrier values are calculated to be 43 and 45 kJ/mol for two cases (two O atoms of the iron site) as mentioned above. The desorption barriers are 62 and 64 kJ/mol if water desorbs from the surface. When formaldehyde is absent on the surface, desorption barrier value for water is computed as 101 kJ/mol.

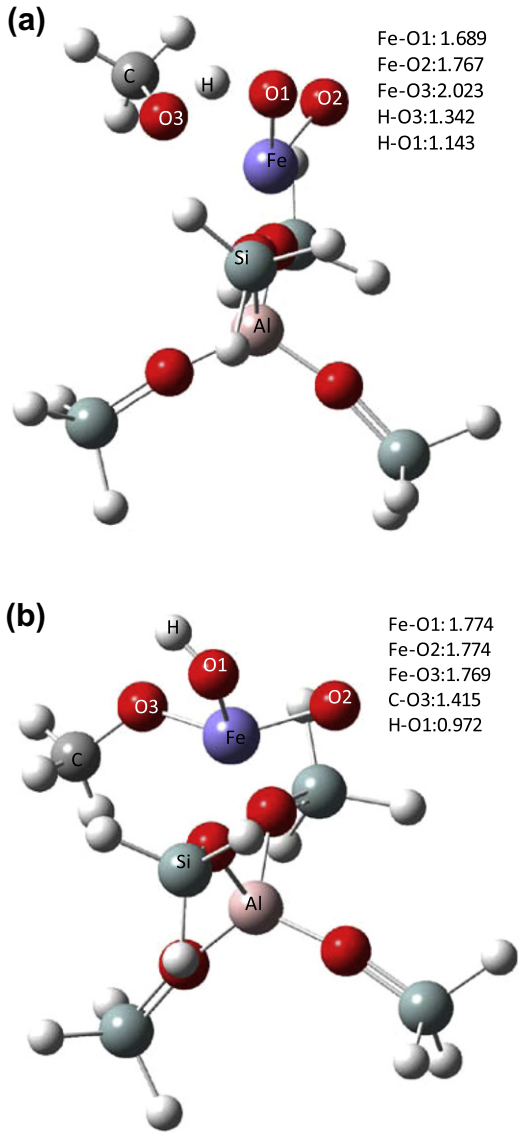

Fig. 6. (a) TS and (b) EG proton transfer from the OH to form grafted species (step B3a) (distance values in units of angstroms).

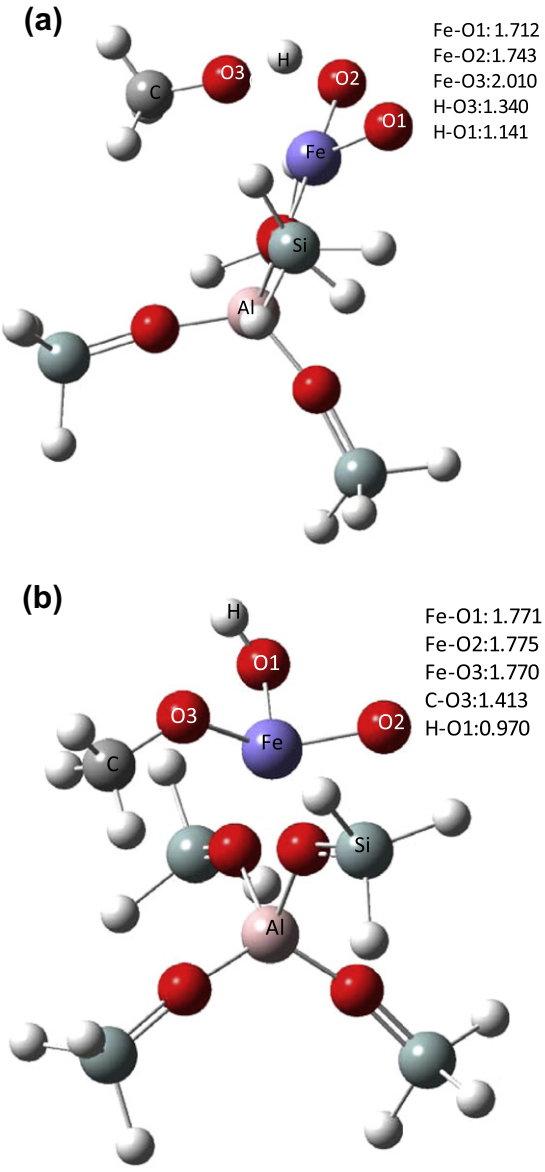

Fig. 7. (a) TS and (b) EG proton transfer from the OH to form grafted species (step B3b) (distance values in units of angstroms).

4. Discussion

The catalytic oxidation of methanol to formaldehyde by N_2O on $[Fe]^{1+}$ and $[FeO]^{1+}$ sites in Fe–ZSM-5 zeolite has been investigated theoretically in this study. The SM number of 6 computed in this study for the $[Fe]^{1+}$– and $[FeO]^{1+}$–ZSM-5 clusters is the same as the SM number used in the literature [16,17,19,36,39,63–67]. A 5T ZSM-5 cluster model was used to produce formaldehyde from methanol by N_2O in this study since very similar structural and energetic properties of the several adsorption complexes have been achieved in both small 5T and large 83T ZSM-5 cluster models [74], as mentioned in Section 2. Tables 1 and 2 report the Mulliken atomic charges and spin densities, and electron configurations of iron atoms of the cluster for all steps for EG and TS geometries, respectively. As can be seen from these tables, the iron atoms have a high spin density, which indicates that the unpaired electrons are localized on iron atoms. Furthermore, the atomic charges of iron atoms for the clusters after the reactions are somewhat higher than those of the initial ZSM-5 clusters, which show a more positive character on iron atoms in the cluster during the reactions in comparison to the initial ZSM-5 clusters.

Fig. 10 shows a summary the calculated reaction energy diagram (including ZPE corrections) for the oxidation of methanol to formaldehyde by N_2O over the sites such as $[Fe]^{1+}$ and $[FeO]^{1+}$ in Fe–ZSM-5 zeolite. Activation barriers for the respective reaction steps involved in the methanol oxidation to formaldehyde are also tabulated in Table 3. Prior to the methanol oxidation, [Fe] and [Fe–O] sites promote the N_2O decomposition resulting in the formation of [Fe–O] and [O–Fe–O] sites, respectively. The formed extra-framework oxygen species on the ZSM-5 clusters are the reactive centers for the following oxidation of methanol to formaldehyde. Decomposition of N_2O molecule on both $[Fe]^{1+}$ and $[FeO]^{1+}$ sites has been investigated on the same cluster models and discussed in our previous theoretical studies [39,65].

The most critical reaction for the methanol oxidation is the activation of O–H bond of methanol since dissociation energy of that bond is 435 kJ/mol [6]. In this study, the activation barrier value for the proton transfer from OH of adsorbed methanol on [FeO] site to form grafted species (step A3) is calculated to be 23 kJ/mol. This value is substantially lower than the value of dissociation energy of O–H bond of methanol. In addition, the activation barrier value of

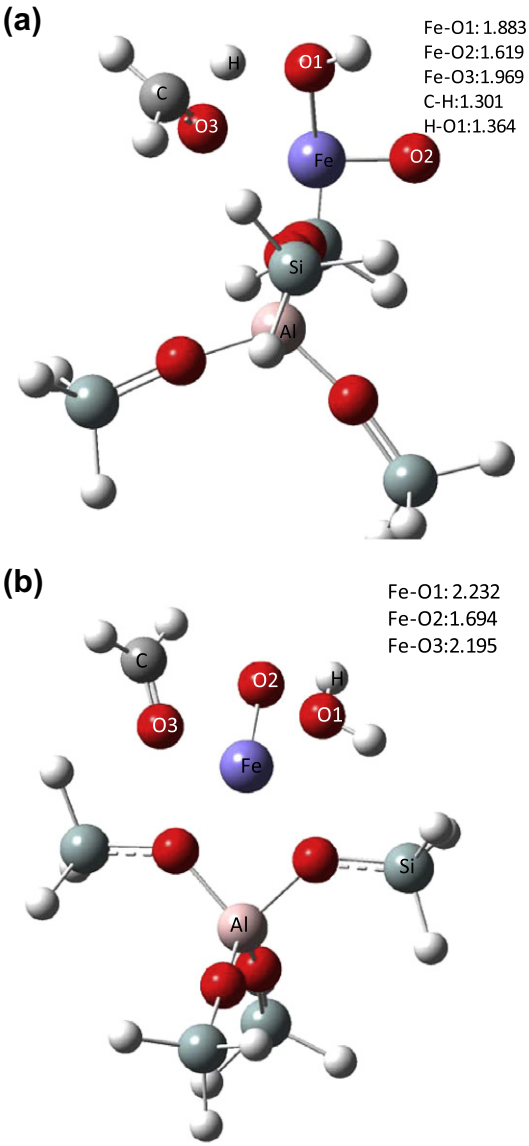

Fig. 8. (a) TS and (b) EG proton transfer CH_3 of metoxy to form formaldehyde and water after step B3a (step B4) (distance values in units of angstroms).

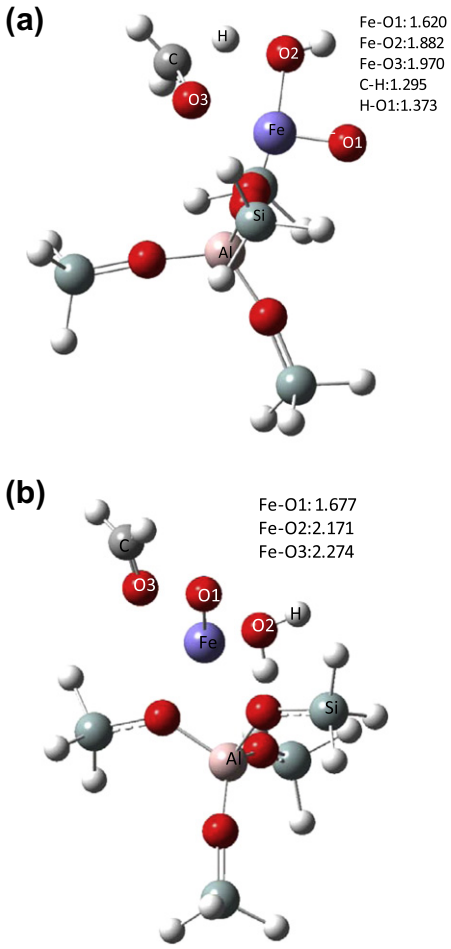

Fig. 9. (a) TS and (b) EG proton transfer CH_3 of metoxy to form formaldehyde and water after step B3b (step B5) (distance values in units of angstroms).

step A3 is somewhat lower than the value of 62 kJ/mol obtained on 3T $[FeO]^{1+}$–ZSM-5 cluster [7]. The difference with the results presented here is probably due to the differences in the computational methodologies used and more specifically to the differences in basis sets used for the description of iron atoms. Moreover, this value is also significantly lower than the theoretical value of 141 kJ/mol for the formation of grafted species on iron-oxo ($[FeO]^{1+}$) with sextet spin state although different basis sets were used for atoms for methanol oxidation [6]. This shows that Fe–ZSM-5 catalyst has a positive effect on methanol oxidation to formaldehyde. In the next step, the activation of grafted species to form formaldehyde and water on the surface (step A4) has required a high energy barrier (E_{act} = 155 kJ/mol). This is probably due to the fact that the formation of grafted species of [HO–Fe–OCH_3] (step A3) is a reaction step which is strongly favored thermodynamically on the site (ΔE = −537 kJ/mol). The activation barrier of this step is somewhat lower than the value (165 kJ/mol) for formaldehyde and water formation from grafted species by using 3T $[FeO]^{1+}$–ZSM-5 cluster [7]. Additionally, the activation barrier value of 155 kJ/mol for step A4 is slightly higher than the value of 145 kJ/mol obtained for formaldehyde formation from the grafted species on iron-oxo structure by Yoshizawa and Kagawa [6]. After the formation of formaldehyde and water on the surface, water firstly desorbs with a desorption barrier value of 81 kJ/mol from the surface since formaldehyde desorption from the surface has a higher desorption barrier (138 kJ/mol). Furthermore, Gibbs free energy changes that were calculated for desorption of water and formaldehyde from the surface [H_2O–Fe–OCH_2] (+35 and +102 kJ/mol, respectively) also indicate this order of desorption. Finally, formaldehyde desorption (step A6) has a desorption value of 127 kJ/mol.

All of the formaldehyde formation paths (steps A1–A6) over $[Fe]^{1+}$ resulted in the formation of a oxygenated $[Fe–O]^{1+}$ species, which can also act as the reactive center for methanol oxidation to formaldehyde by N_2O. These steps are similar to the steps B1–B7 considered for the $[F–O]^{1+}$ site. On the $[O–Fe–O]^{1+}$ site, there are two alternative reactions (steps B3a and B3b) for proton transfer from OH group of adsorbed methanol to form methoxy and hydroxyl species. The step B3a is more favorable reaction when compared to step B3b since it has a lower activation energy barrier and $\Delta G^{\#}$ values than those of step B3b (72, +79 kJ/mol vs. 81, +84 kJ/mol). Although the activation barrier values for these reactions (steps B3a and B3b) are somewhat higher than that of step A3 took place on $[Fe–O]^{1+}$ site, they are substantially lower than the dissociation energy value (435 kJ/mol) [6] for O–H bond of methanol. The activation barriers for the proton transfer from CH_3 group of methoxy species to form formaldehyde and water via steps B4 and B5 are very close to each other (24 and 22 kJ/mol, respectively). Moreover, these values are significantly lower than the value (155 kJ/mol) obtained on $[Fe]^{1+}$ site (step A4) in this

Table 1
Mulliken atomic charges and spin densities and electronic configurations of iron atoms for EG structures of steps.

Clusters/steps	Charge	Spin density	Electron configuration of iron atom
Fe^{1+}–ZSM-5	+0.47	4.811	$[core]4s^{1.07}3d^{6.00}4p^{0.09}$
$[FeO]^{1+}$–ZSM-5	+1.00	4.023	$[core]4s^{0.32}3d^{5.94}4p^{0.06}5p^{0.01}$
$[OFeO]^{1+}$–ZSM-5	+1.14	3.069	$[core]4S^{0.27}3d^{5.97}4p^{0.03}4d^{0.01}$
Step A2	+0.98	4.051	$[core]4S^{0.29}3d^{5.93}4p^{0.06}5p^{0.01}$
Step A3	+1.19	4.189	$[core]4S^{0.25}3d^{5.75}4p^{0.04}5p^{0.01}$
Step A4	+0.93	3.762	$[core]4S^{0.38}3d^{6.05}4p^{0.03}5S^{0.01}$
Step A5	+0.49	4.860	$[core]4S^{1.00}3d^{6.05}4p^{0.08}$
$[CH_2O$–Fe]–ZSM-5			
Step B2	+1.15	3.088	$[core]4S^{0.28}3d^{5.93}4p^{0.02}4d^{0.01}$
Step B3a	+1.26	3.318	$[core]4S^{0.28}3d^{5.76}4p^{0.02}4d^{0.01}5p^{0.01}$
Step B3b	+1.26	3.314	$[core]4S^{0.28}3d^{5.76}4p^{0.02}4d^{0.01}5p^{0.01}$
Step B4	+1.00	4.028	$[core]4S^{0.28}3d^{5.91}4p^{0.03}5p^{0.01}$
Step B5	+0.99	4.049	$[core]4S^{0.29}3d^{5.92}4p^{0.05}5p^{0.01}$
Step B6	+0.98	4.081	$[core]4S^{0.30}3d^{5.93}4p^{0.07}5p^{0.01}$
$[H_2O$–Fe–O]–ZSM-5			

Table 2
Mulliken atomic charges and spin densities and electronic configurations of iron atoms for TS structures of steps.

Steps	Charge	Spin density	Electron configuration of iron atom
Step A3	+1.05	4.133	$[core]4S^{0.29}3d^{5.83}4p^{0.04}5p^{0.01}$
Step A4	+1.00	3.854	$[core]4S^{0.31}3d^{6.01}4p^{0.03}5S^{0.01}$
Step B3a	+1.15	3.158	$[core]4S^{0.30}3d^{5.85}4p^{0.02}4d^{0.01}5p^{0.01}$
Step B3b	+1.18	3.219	$[core]4S^{0.29}3d^{5.83}4p^{0.02}4d^{0.01}5p^{0.01}$
Step B4	+1.20	3.201	$[core]4S^{0.27}3d^{5.85}4p^{0.02}4d^{0.01}5p^{0.01}$
Step B5	+1.19	3.201	$[core]4S^{0.27}3d^{5.86}4p^{0.02}4d^{0.01}5p^{0.01}$

study. The reason for this difference between the activation barriers of steps A3 and B3 (grafted species formation) and steps A4 and B4,5 (formaldehyde formation) might be that in transition state modes that have lower activation barriers the distance of H–O is much greater than those of other modes having higher activation barriers. After the formations of formaldehyde and water, formaldehyde molecules firstly desorb with desorption barrier values of

Table 3
Activation barriers of all steps for direct oxidation of methanol to formaldehyde by N_2O on Fe–ZSM-5 zeolite (values in units of kJ/mol).

Steps	$[Fe]^{1+}$ site	$[FeO]^{1+}$ site
Step A1. N_2O decomposition	18	
Step A2. Methanol adsorption	0	
Step A3. Proton transfer from the OH to form grafted species	23, 62[a]	
Step A4. Proton transfer from the metoxy to form formaldehyde and water	155, 165[a]	
Step A5. Desorption of water	81	
Step A6. Desorption of formaldehyde	127	
Step B1. N_2O decomposition		113
Step B2. Methanol adsorption		0
Step B3a. Proton transfer from the OH to form grafted species		72
Step B3b. Proton transfer from the OH to form grafted species		81
Step B4. Proton transfer metoxy to form formaldehyde and water after step B3a		24
Step B5. Proton transfer metoxy to form formaldehyde and water after step B3b		22
Step B6. Desorption of formaldehyde		43, 45
Step B7. Desorption of water		101

[a] Liang et al. [7] 3T cluster, $[(SiH_3)_2AlO_2(OH)_2(FeO)]$.

43 and 45 kJ/mol from the surface $[H_2O$–O–Fe–$OCH_2]$, since water desorptions from the surface have higher desorption barriers (62 and 64 kJ/mol). Finally, water desorption (step A6) has a desorption value of 101 kJ/mol).

Wood et al. [42] have reported in their experimental study on Fe–ZSM-5 catalyst that the pair of bands at 2921 and 2824 cm^{-1} was assigned to the asymmetric and symmetric C–H stretching for Fe-bound methoxy groups. In this study, corresponding frequency values are calculated to be 2943, 2881 cm^{-1} and 2960, 2892 cm^{-1} for grafted species including methoxy and hydroxyl on Fe–ZSM-5 clusters (steps A3 and B3), respectively. The stretching frequencies of O–H for surface hydroxyl are computed as 3724 and 3626 cm^{-1} for the same steps, respectively. The band at 3673 cm^{-1} was assigned to hydroxyl group bonded to extra-framework Fe where the study was done on Fe/Al-MFI catalyst [42],

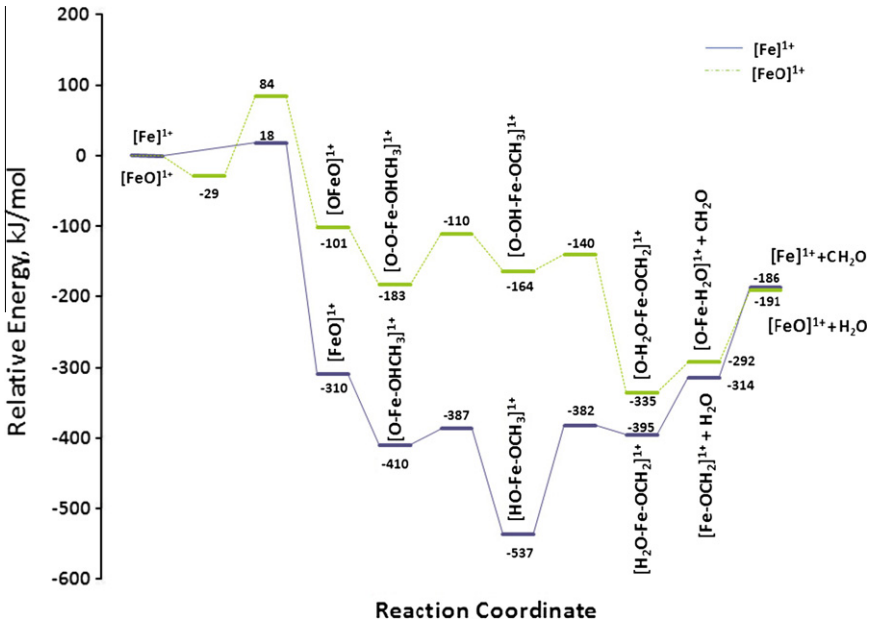

Fig. 10. Relative energy profile (including ZPE corrections) for direct methanol oxidation to formaldehyde on $[Fe]^{1+}$ and $[Fe–O]^{1+}$ sites in Fe–ZSM-5 (steps A1–A6 and B1–B7).

based on similar bands on FeOOH due to OH coordinated Fe [83,84]. It has also been reported that a series of bands were observed at lower energies with the frequencies of 1460, 1434, and 1413 cm^{-1} which were then assigned to methoxy CH-bending vibrations [42]. The equivalent vibrational frequencies are computed as 1445, 1439, 1429 cm^{-1} and 1435, 1433, 1420 cm^{-1} for equilibrium geometries of steps A3 and B3 including grafted species in this study. These bands are also in the region of the spectrum projected for methoxy bending vibrations of C–H [85]. Consequently, theoretical frequencies calculated for surface grafted species in the present study are in a good agreement with the experimental data [42] mentioned above for methoxy and hydroxyl species on Fe/Al-MFI catalyst. Additionally, it has been also reported by Wood et al. [42] that the intensities of the O–H bands are much greater than those of the corresponding methoxy C–H bands. A parallel observation has been previously reported for the interaction of methanol with ZSM-5 [86]. In the same way, IR intensities for the O–H stretching frequencies are significantly greater than those of C–H stretching frequencies of surface methoxy species in the present study. Other vibrational frequencies of equilibrium geometries for catalytic cycle steps are tabulated in Table 4.

Table 4
Vibrational frequencies of equilibrium geometries for catalytic steps.

Step	Type of frequency		Frequency
Step A2	Fe–O	Streching	881
	C–O	Streching	981
	H of OH	Rocking	1057
	O–H	Streching	3671
Step A3	H of OH	Rocking	545
	OH	Streching	704
	C–O	Streching	1105
	O–H	Streching	3724
Step A4	H of CH_2O	Wagging	850
	H of CH_2O	Rocking	1133
	C–O	Streching	1240
	H of CH_2O	Scissoring	1453
	H of H_2O	Scissoring	1537
	Hs of CH_2O	Symmetrical streching	2907
	Hs of CH_2O	Anti-symmetrical streching	3006
	H of H_2O	Streching	3091, 3709
Step A5 [CH_2O–Fe]–ZSM-5	H of CH_2O	Wagging	743
	H of CH_2O	Rocking	1117
	C–O	Streching	1155
	H of CH_2O	Scissoring	1440
	Hs of CH_2O	Symmetrical streching	2952
	Hs of CH_2O	Anti-symmetrical streching	3059
Step B2	O–O	Anti-symmetrical streching	585
	O–O	Symmetrical streching	855
	C–O	Streching	986
	H of OH	Rocking	1048
	O–H	Streching	3649
Step B3	H of OH	Rocking	416
	O–O(OH)	Anti-symmetrical streching	640
	O–O(OCH_3)	Symmetrical streching	546
	OH	Streching	685
	C–O	Streching	1036
	O–H	Streching	3633
Step B4	Fe–O	Streching	835
	H of CH_2O	Rocking	1224
	H of CH_2O	Scissoring	1453
	H of H_2O	Scissoring	1536
	C–O	Streching	1698
	Hs of CH_2O	Symmetrical streching	2877
	Hs of CH_2O	Anti-symmetrical streching	2990
	H of H_2O	Streching	3472, 3668
Step B6 [H_2O–Fe]–ZSM-5	Fe–O	Streching	896
	H of H_2O	Scissoring	1584
	H of H_2O	Streching	3305, 3719

The TD-DFT computed UV–vis spectra for the structure containing Fe–metoxy and Fe–OH reveal absorption bands at max 157 nm in the range of 140–180 nm on $[Fe]^{1+}$ site. The UV–vis bands for the metoxy species on the $[Fe–O]^{1+}$ site were computed to be max 293 nm in the range of 250–350 nm and max 216 nm in the range of 200–250 nm, respectively. The excited state energy of spectra for $[Fe]^{1+}$ site is significantly higher than that of spectra for $[Fe–O]^{1+}$ site. This is probably due to the fact that surface metoxy species on $[Fe]^{1+}$ site is much more thermodynamically stable than those on $[Fe–O]^{1+}$ site.

In summary, the fundamental result of this study is that the interaction of the $[Fe–O]^{1+}$ site with methanol to produce formaldehyde by N_2O is more energetically favored that involving the mononuclear iron site of $[Fe]^{1+}$ in ZSM-5. The most important difference between these two sites is that in the case of the $[Fe]^{1+}$ site, a reaction is present that leads to the formation of the thermodynamically highly stable grafted OH and methoxy (OCH_3) species. The activation barrier for formaldehyde formation on $[O–Fe–O]^{1+}$ site is considerably lower than that of the reaction on $[Fe–O]^{1+}$ site. The reason of this might be explained that grafted species formed on $[Fe]^{1+}$ site is much more thermodynamically stable than that on $[FeO]^{1+}$ site. Moreover, there seems to be a great consistency between the overall heat of reaction values for direct oxidation of methanol to formaldehyde by N_2O on $[Fe]^{1+}$ and $[FeO]^{1+}$ sites of Fe–ZSM-5 clusters (−186 and −191 kJ/mol, respectively). The vibrational frequencies for grafted species on the surface are also in line with the experimental values. Whereas the theoretical results obtained in this study clearly indicate the significant role of $[Fe–O]^{1+}$ site in Fe–ZSM-5 catalyst in the catalytic oxidation of methanol to formaldehyde by N_2O, obviously there is a need to also study more extensively other sites such as $[Fe]^{2+}$, $[FeO]^{2+}$ and $[FeO-Fe]^{2+}$ of Fe–ZSM-5 for this reaction.

5. Conclusion

The elementary reaction steps involved in the catalytic methanol oxidation to formaldehyde by N_2O over iron sites in Fe–ZSM-5 zeolite represented by a $[(SiH_3)_4AlO_4(Fe)$ or $(FeO)]$ clusters model have been investigated by means of DFT calculations. The major difference between these two sites is that in the case of the $[Fe]^{1+}$ site, a reaction is present that leads to the formation of the thermodynamically highly stable grafted OH and methoxy (OCH_3) species. The vibrational frequencies for grafted species on the surface are in good agreement with the experimental values. According to the results obtained in this study, $[Fe–O]^{1+}$ site in Fe–ZSM-5 catalyst has a unique role on the catalytic direct oxidation of methanol to formaldehyde by N_2O.

Acknowledgment

The numerical calculations reported in this paper were partially performed at TUBITAK ULAKBIM, High Performance and Grid Computing Center (TR-Grid e-Infrastructure).

References

[1] A. English, J. Brown, J. Rovner, S. Davies, Kirk–Othmer Encyclopedia of Chemical Technology, third ed., vol. 16, Wiley, Hoboken, NJ, 2005. p. 299.

[2] H. Robert, G. George, C. Seaman, Kirk–Othmer Encyclopedia of Chemical Technology, third ed., vol. 12, Wiley, Hoboken, NJ, 2005. p. 107.
[3] M.J. Louwerse, P. Vassilev, E.J. Baerends, J. Phys. Chem. A. 112 (2008) 1000.
[4] T. Ohta, T. Kamachi, Y. Shiota, K. Yoshizawa, J. Org. Chem. 66 (2001) 4122.
[5] Y. Xie, F. Dong, S. Heinbuch, J.J. Rocca, E.R. Berstein, J. Chem. Phys. 130 (2009) 114306-1.
[6] K. Yoshizawa, Y. Kagawa, J. Phys. Chem. A 104 (2000) 9347.
[7] W.Z. Liang, A.T. Bell, M. Head-Gordon, A.K. Chakraborty, J. Phys. Chem. B 108 (2004) 4362.
[8] E.J.M. Hensen, Q. Zhu, R.A.J. Janssen, P.C.M.M. Magusin, P.J. Kooyman, R.A. van Santen, J. Catal. 233 (2005) 123.
[9] E.J.M. Hensen, Q. Zhu, R.A. van Santen, J. Catal. 233 (2005) 136.
[10] A.S. Kharitonov, T.N. Aleksandrova, G.I. Panov, V.I. Sobolev, G.A. Sheveleva, E.A. Paukshtis, Kinet. Catal. 35 (1994) 270.
[11] V.I. Sobolev, A.S. Kharitonov, Y.A. Paukshtis, G.I. Panov, J. Mol. Catal. 84 (1993) 117.
[12] A.M. Volodin, V.A. Bolshov, G.I. Panov, J. Phys. Chem. 98 (1994) 7548.
[13] V.S. Chernyavsky, L.V. Pirutko, A.K. Uriarte, A.S. Kharitonov, G.I. Panov, J. Catal. 245 (2007) 466.
[14] V.N. Parmon, G.I. Panov, A. Uriarte, A.S. Noskov, Catal. Today 100 (2005) 100.
[15] K.A. Dubkov, V.I. Sobolev, E.P. Talsi, M.A. Rodkin, N.H. Watkins, A.A. Shteinman, G.I. Panov, J. Mol. Catal. A 123 (1997) 155.
[16] J.A. Ryder, A.K. Chekraborty, A.T. Bell, J. Catal. 220 (2003) 84.
[17] K. Yoshizawa, Y. Shiota, Y. Kagawa, T. Yamabe, J. Phys. Chem. B 104 (2000) 734.
[18] K. Yoshizawa, Y. Shiota, Y. Yamabe, J. Am. Chem. Soc. 121 (1999) 147.
[19] Y. Shiota, K. Suzuki, K. Yoshizawa, Organometallics 25 (2006) 3118.
[20] N.A. Kachurovskaya, G.M. Zhidomirov, E.J.M. Hensen, R.A. van Santen, Catal. Lett. 86 (2003) 25.
[21] F. Kapteijn, J. Rodreiguez-Mirasol, J.A. Moulijn, Appl. Catal. B 9 (1996) 25.
[22] F. Kapteijn, G. Marb, J. Rodriguez-Mirasol, J.A. Moulijn, J. Catal. 167 (1997) 256.
[23] E.M. El-Malki, R.A. van Santen, W.M.H. Sachtler, J. Catal. 196 (2000) 212.
[24] B.R. Wood, J.A. Reimer, A.T. Bell, M.T. Janicke, K.C. Ott, J. Catal. 224 (2004) 148.
[25] Q. Zhu, B.L. Mojet, E.J.M. Janssen, J. van Grondelle, P.C.M.M. Magusin, R.A. van Santen, Catal. Lett. 81 (2002) 205.
[26] G.D. Pirngruber, P.K. Roy, R. Prins, J. Catal. 246 (2007) 147.
[27] G.D. Pirngruber, M. Luechinger, P.K. Roy, A. Cecchetto, P. Smirniotis, J. Catal. 224 (2004) 429.
[28] J.C. Groen, A. Brückner, E. Berrier, L. Maldonado, J.A. Moulijin, J.P. Ramirez, J. Catal. 243 (2006) 212.
[29] R.S. da Cruz, A.J.S. Mascarenhas, H.M.C. Andrade, Appl. Catal. B 18 (1998) 223.
[30] K.A. Dubkov, N.S. Ovannesyan, A.A. Shteinman, E.V. Starokon, G.I. Panov, J. Catal. 207 (2002) 341.
[31] G.I. Panov, A.K. Uriarte, M.A. Rodkin, V.I. Sobolev, Catal. Today 41 (1998) 365.
[32] N. Hansen, A. Heyden, A.T. Bell, F.J. Keil, J. Catal. 248 (2007) 213.
[33] A. Heyden, A.T. Bell, F.J. Keil, J. Catal. 233 (2005) 26.
[34] A.L. Yakovlev, G.M. Zhidomirov, R.A. van Santen, Catal. Lett. 75 (2001) 45.
[35] A.L. Yakovlev, G.M. Zhidomirov, R.A. van Santen, J. Phys. Chem. B 105 (2001) 12297.
[36] A. Heyden, B. Peters, A.T. Bell, F.J. Keil, J. Phys. Chem. B 109 (2005) 1857.
[37] J.A. Ryder, A.K. Chakraborty, A.T. Bell, J. Phys. Chem. B 106 (2002) 7059.
[38] K. Yoshizawa, T. Yumura, Y. Yoshihito, T. Yamabe, Bull. Chem. Soc. Jpn. 73 (2000) 29.
[39] M.F. Fellah, I. Onal, Catal. Today 137 (2007) 410.
[40] K. Yoshizawa, T. Yumura, Y. Shiota, T. Yamabe, Bull. Chem. Soc. Jpn. 73 (2000) 29.
[41] N. Hansen, A. Heyden, A.T. Bell, F.J. Keil, J. Phys. Chem. C 111 (2007) 2092.
[42] B.R. Wood, J.A. Reimer, A.T. Bell, M.T. Janicke, K.C. Ott, J. Catal. 225 (2004) 300.
[43] E.J.M. Hensen, Q. Zhu, P.H. Liu, K.J. Chao, R.A. van Santen, J. Catal. 226 (2004) 466.
[44] G.I. Panov, CATTECH 4 (2000) 18.
[45] M.F. Fellah, R.A. Van Santen, I. Onal, J. Phys. Chem. C 113 (2009) 15307.
[46] A. Zecchina, F. Geobaldo, C. Lamberti, S. Bordiga, G. Turnes Palomino, C. Otero Arean, Catal. Lett. 42 (1996) 25.
[47] A.A. Battiston, J.H. Bitter, F.M.F. de Groot, A.R. Overweg, O. Stephan, J.A. van Bokhoven, P.J. Kooyman, C. van der Spek, G. Vanko, D.C. Koningsberger, J. Catal. 213 (2003) 251.
[48] A. Zecchina, M. Rivallan, G. Berlier, C. Lamberti, G. Ricciardi, Phys. Chem. Chem. Phys. 9 (2007) 3483.
[49] K. Krishna, M. Makkee, Catal. Today 114 (2006) 23.
[50] R.Q. Long, R.T. Yang, Catal. Lett. 74 (2001) 201.
[51] M. Schwidder, M.S. Kumar, K. Klementiev, M.M. Pohl, A. Brückner, W. Grünert, J. Catal. 231 (2005) 314.
[52] F. Heinrich, E. Schmidt, M. Menzel, W. Grünert, J. Catal. 212 (2002) 157.
[53] S. Brandenberger, O. Kröcker, A. Tissler, R. Althoff, Appl. Catal. B 95 (2010).
[54] A.M. Volodin, G.M. Zhidomirov, K.A. Dubkov, E.J.M. Hensen, R.A. van Santen, Catal. Today 110 (2005) 247.
[55] V.I. Sobolev, G.I. Panov, A.S. Kharitonov, V.N. Romannikov, A.M. Volodin, K.G. Ione, J. Catal. 139 (1993) 435.
[56] G.I. Panov, V.I. Sobolev, K.A. Dubkov, V.N. Parmon, N.S. Ovanesyan, A.E. Shilov, A.A. Shteinman, React. Kinet. Catal. Lett. 61 (1997) 251.
[57] N.S. Ovanesyan, A.A. Steinman, V.I. Sobolev, K.A. Dubkov, G.I. Panov, Kinet. Katal. 38 (1998) 863.
[58] H. Xia, K. Sun, Z. Liu, Z. Feng, P. Ying, C. Li, J. Catal. 270 (2010) 103.
[59] M.S. Kumar, M. Schwidder, W. Grünert, A. Brückner, J. Catal. 227 (2004) 384.
[60] R. Joyner, M. Stockenhuber, J. Phys. Chem. B 103 (1999) 5963.
[61] M. Schwidder, M.S. Kumar, A. Brückner, W. Grünert, Chem. Commun. (2005) 805.
[62] J. Jia, Q. Sun, B. Wen, L.X. Chen, W.M.H. Sachtler, Catal. Lett. 82 (2002) 7.
[63] K. Yoshizawa, Y. Shiota, T. Kamachi, J. Phys. Chem. B 107 (2003) 11404.
[64] M.F. Fellah, I. Onal, Turkish J. Chem. 33 (2009) 333.
[65] M.F. Fellah, I. Onal, R.A. van Santen, J. Phys. Chem. C 114 (2010) 12580.
[66] M.F. Fellah, I. Onal, J. Phys. Chem. C 114 (2010) 3042.
[67] A. Heyden, N. Hansen, A.T. Bell, F.J. Keil, J. Phys. Chem. B 110 (2006) 17096.
[68] W. Kohn, L. Sham, J. Phys. Rev. 140 (1965) A1133.
[69] M.J. Frisch, G.W. Trucks, H.B. Schlegel, G.E. Scuseria, M.A. Robb, J.R. Cheeseman, G. Scalmani, V. Barone, B. Mennucci, G.A. Petersson, H. Nakatsuji, M. Caricato, X. Li, H.P. Hratchian, A.F. Izmaylov, J. Bloino, G. Zheng, J.L. Sonnenberg, M. Hada, M. Ehara, K. Toyota, R. Fukuda, J. Hasegawa, M. Ishida, T. Nakajima, Y. Honda, O. Kitao, H. Nakai, T. Vreven, J.A. Montgomery Jr., J.E. Peralta, F. Ogliaro, M. Bearpark, J.J. Heyd, E. Brothers, K.N. Kudin, V.N. Staroverov, R. Kobayashi, J. Normand, K. Raghavachari, A. Rendell, J.C. Burant, S.S. Iyengar, J. Tomasi, M. Cossi, N. Rega, J.M. Millam, M. Klene, J.E. Knox, J.B. Cross, V. Bakken, C. Adamo, J. Jaramillo, R. Gomperts, R.E. Stratmann, O. Yazyev, A.J. Austin, R. Cammi, C. Pomelli, J.W. Ochterski, R.L. Martin, K. Morokuma, V.G. Zakrzewski, G.A. Voth, P. Salvador, J.J. Dannenberg, S. Dapprich, A.D. Daniels, Ö. Farkas, J.B. Foresman, J.V. Ortiz, J. Cioslowski, D.J. Fox, Gaussian, Inc., Wallingford, CT, 2009.
[70] A.D. Becke, Phys. Rev. B 38 (1988) 3098.
[71] A.D. Becke, M.R. Roussel, Phys. Rev. A 39 (1989) 3761.
[72] C. Lee, W. Yang, R.G. Parr, Phys. Rev. B 37 (1988) 785.
[73] N.A. Kachurovskaya, G.M. Zhidomirov, E.J.M. Hensen, R.A. van Santen, J. Phys. Chem. B 108 (2004) 5944.
[74] M.F. Fellah, J. Phys. Chem. C 115 (2011) 1940.
[75] X. Rozanska, X. Saintigny, R.A. van Santen, F. Hutschka, J. Catal. 202 (2001) 141.
[76] X. Rozanska, R.A. van Santen, F. Hutschka, J. Hafner, J. Am. Chem. Soc. 123 (2001) 7655.
[77] A.M. Vos, X. Rozanska, R.A. Schoonheydt, R.A. van Santen, F. Hutschka, J. Hafner, J. Am. Chem. Soc. 123 (2001) 2799.
[78] H. Lermer, M. Draeger, J. Steffen, K.K. Unger, Zeolites 5 (1985) 131.
[79] M.W. Wong, Chem. Phys. Lett. 256 (1996) 391.
[80] R.S. Mulliken, J. Chem. Phys. 23 (1955) 1833.
[81] E.D. Glendening, A.E. Reed, J.E. Carpenter F. Weinhold, NBO, Version 3.1, Theoretical Chemistry Institute, Gaussian Inc., University of Wisconsin, Madison, WI.
[82] H.B. Schlegel, J. Comput. Chem. 3 (1982) 214.
[83] T. Ishikawa, S. Nitta, S. Kondo, J. Chem. Soc., Faraday Trans. 82 (1986) 2401.
[84] T. Ishikawa, W.Y. Cai, K. Kandori, J. Chem. Soc., Faraday Trans. 88 (1992) 1173.
[85] T.R. Forester, R.F. Howe, J. Am. Chem. Soc. 109 (1987) 5076.
[86] X.Z. Jiang, J. Mol. Catal. 121 (1997) 63.